Dual 3L-NPC Converter System With Improved Power Quality for Bipolar DC Distribution

Bowei Li, *Graduate Student Member, IEEE*, Xuesong Wu, *Graduate Student Member, IEEE*, Gregory J. Kish, *Senior Member, IEEE*, and Yunwei Ryan Li, *Fellow, IEEE*

***Abstract*—Three-level neutral point clamped (3L-NPC) converters are a favorable candidate for the grid interfacing converter stage in bipolar dc distribution systems. This article proposes the use of dual 3L-NPCs where, by virtue of connecting their ac ports in a differential fashion across a center-tapped transformer winding, two main benefits can be realized: 1) full bipolar voltage balancing capability that can accommodate any degree of imbalance between two dc poles, and 2) improved dc-side power quality in terms of reduced ripples in the pole voltages and currents. The proposed converter system also avoids the reliance on more complex zigzag transformer arrangements used in prior art. Detailed theoretical analyses of the pole voltage balancing and the ripple reduction mechanisms are conducted, with the results guiding the development of a suitable control strategy. The advantages of the proposed scheme and the correctness of the theoretical analyses are validated through both simulation and experimental results.**

***Index Terms*—Bipolar dc distribution, dc voltage unbalance, neutral point voltage balancing, three-level neutral point clamped (3L-NPC) converter.**

I. Introduction

DC DISTRIBUTION technology is rising in prominence due to ongoing advancements in power electronics [1]. Power electronic converters are the key building blocks to realize dc distribution system architectures that offer higher efficiency, faster response, and better current carrying capacity relative to legacy ac systems [2], [3]. Benefitting from the successful application of high voltage dc transmission over the past decades, we are witnessing the emergence of medium voltage (MV) and low voltage dc distribution systems as they can readily integrate the growing number of distributed energy resources (DERs) and dc loads. DC distribution systems can also avoid unnecessary ac-dc conversion stages, yielding reduced conversion losses and capital cost as well as potentially simplified operation [4].

Unipolar and bipolar configurations are two common options for building a dc distribution system. The bipolar configuration offers more available poles and voltage levels relative to unipolar implementation, and therefore is viewed as more promising by virtue of the higher flexibility and reliability [5]. For bipolar dc distribution system, one major challenge is operating under asymmetrical dc poles caused by unbalanced loads or DERs. As shown in Fig. 1, when the required powers of two poles are unequal, a dc-side neutral balancing current (denoted by i) must be accommodated by the distribution converter for bipolar voltage balancing. Otherwise, the pole voltages may become uncontrolled and unbalanced, adversely affecting the conversion efficiency, or even stability and safety of the entire system [6].

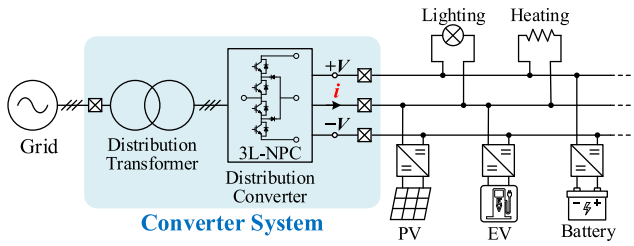

Fig. 1. Bipolar DC distribution architecture with grid interfacing converter system.

The distribution converter plays a key role in solving the dc-side asymmetrical operation problem. Compared to a two-level voltage source converter (2L-VSC), a three-level neutral point clamped converter (3L-NPC) is selected as the distribution converter in Fig. 1 in view of its advantages of more voltage levels, lower total harmonic distortion and switching frequency, higher efficiency, and reduced stress across switches [7], [8], [9]. Since a split-dc bus structure is necessary for the bipolar configuration, the split dc-link capacitors of the 3L-NPC render it a natural candidate for the distribution converter. Moreover, the 3L-NPC inherently provides a certain level of voltage balancing capability for asymmetrical operation of dc poles [10], [11]. Besides, as a successful topology of multilevel converter, the 3L-NPC is the preferred choice in many industrial MV applications [12]. Compared to the modular multilevel converter (MMC), which is another prominent multilevel converter, the 3L-NPC has a simpler structure and lower cost, making it a promising candidate for the medium voltage dc (MVDC) distribution system. The 3L-NPC also has wide industry acceptance and accessibility like the 2L-VSC [13], which is beneficial to the future construction and popularization of dc distribution grids.

Many bipolar dc distribution schemes based on 3L-NPC have been proposed in recent years and some are reported to already be adopted in pilot MVDC systems. One example is the ANGLE-DC project, a ±27 kV bipolar MVDC demonstration project in

Manuscript received 20 March 2024; revised 28 June 2024; accepted 5 August 2024. Date of publication 12 August 2024; date of current version 7 October 2024. Recommended for publication by Associate Editor Z. Zhang. *(Corresponding author: Bowei Li.)*

The authors are with the Department of Electrical Computer Engineering, University of Alberta, Edmonton, AB T6G 2R3, Canada (e-mail: bli4@ualberta.ca; xuesong3@ualberta.ca; gkish@ualberta.ca; yunwei.li@ualberta.ca).

Color versions of one or more figures in this article are available at https://doi.org/10.1109/TPEL.2024.3441610.

Digital Object Identifier 10.1109/TPEL.2024.3441610

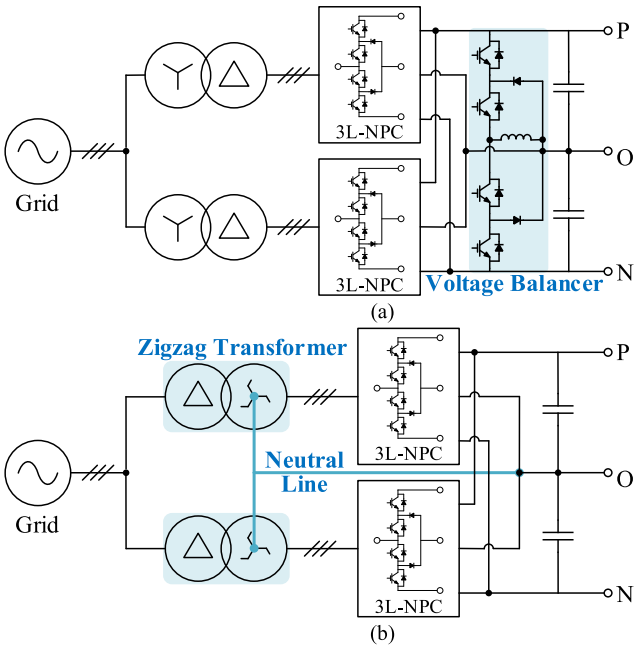

Fig. 2. Bipolar DC distribution schemes for high-power applications. (a) Paralleled 3L-NPC converters with a voltage balancer. (b) Paralleled 3L-NPC converters with zigzag transformers and a neutral line.

the U.K. [14], [15]. In this project, cascaded 3L-NPC converters are used together with multiwinding transformers to form the overall distribution converter system. This configuration allows full control of the power injections at each dc pole via independent control of the cascaded converters. However, for high power applications, a paralleled connection of the converters would offer better adaptability to higher currents as they can be distributed between the paralleled converters.

Fig. 2(a) shows a converter system based on two paralleled 3L-NPC converters. Since the 3L-NPC converters are validated to have inherent but limited voltage balance operation area [10], [16], additional circuits such as a fourth converter leg or a dedicated voltage balancer (VB) are typically added to ensure dc pole voltage balance under any load conditions [10], [17], which inevitably increases overall system cost, losses, and complexity. In contrast, an improved 3L-NPC converter system based on a zigzag transformer was recently proposed in [16] that can provide full bipolar voltage balancing capability without adding an extra VB. This is done by multitasking the zigzag windings to carry the dc-side neutral balancing current, without imposing any dc flux in the transformer core. Relying on the saturation-free advantages under dc offset currents, the zigzag transformers are validated to be able to realize bipolar dc distribution systems with many kinds of converters, e.g., MMC [18], 2L-VSC [19], dual-active bridge converter [20].

For high-power dc distribution systems, two sets of 3L-NPC converters and zigzag transformers in [16] can be used in parallel, as shown in Fig. 2(b). However, this arrangement requires two separate zigzag transformers that are more complex in design than the conventional transformers, leading to higher cost. Additionally, despite the efforts in keeping pole voltages balanced, these schemes all inevitably suffer from ac ripple issues for the dc pole voltages. According to the extensive studies on the neutral point (NP) voltage balancing problem of 3L-NPC in the past [21], [22], [23], [24], [25], [26], [27], [28], these undesired capacitor voltage ripples are caused by low-order harmonics in the NP current, which is an inherent character of the 3L-NPC [21]. For the bipolar dc distribution system, the pole voltage ripples will deteriorate the power quality of the pole currents and impose increased stress on the semiconductor switches. A number of pulsewidth modulation (PWM) methods have been proposed to reduce the capacitor voltage ripples, which can mainly be categorized into space vector PWM methods [22], [23], [24] and carrier-based PWM methods [25], [26], [27]. They generally take the same approach of adding zero sequence voltage to the ac terminal of the 3L-NPC [28]. However, these PWM methods all come with some challenges such as increased computation cost and switching losses, the need for additional measurements, and potential saturation of the modulation signals.

To simultaneously tackle the challenges of 1) pole voltage imbalance caused by the dc-side asymmetrical operation, and 2) pole voltage ripples caused by low-order harmonics inherent to 3L-NPC, this article proposes a dual 3L-NPC converter system for bipolar dc distribution. By exploiting a center-tapped transformer and a neutral line, the proposed converter system can inject the necessary zero sequence dc balancing currents via the common center-tap point, thereby acquiring full bipolar voltage balancing capability. Compared to Fig. 2(b), the proposed scheme only requires one three-winding transformer, offering a simpler structure relative to multiple zigzag transformers. By capitalizing on differential operation of dual 3L-NPC converters, the proposed scheme also eliminates odd multiples of the third harmonic in the total NP current, thereby gaining improved dc-side power quality in terms of ripple reduction. Compared to the aforementioned PWM methods for ripple reduction, the proposed scheme neither suffer their disadvantages nor increase the control complexity. Besides, the proposed dual 3L-NPC converter system is suitable for high power applications as large currents can be divided between two converters. The main contributions of this article are as follows.

1) A dual 3L-NPC converter system with a center-tapped transformer is proposed for high-power bipolar dc distribution. Compared to existing schemes, the proposed scheme acquires full bipolar voltage balancing capability through a simpler transformer arrangement and realizes improved dc-side power quality via the differential operation of dual converters.
2) A detailed theoretical analysis of the operation of the proposed dual 3L-NPC system is conducted, with the results guiding the design of a control strategy that ensures pole voltage balance under all the load conditions while concurrently reducing the ripples for the pole voltages and currents.

The rest of this article is organized as follows. Section II first presents the structure of the proposed converter system, then the features of the center-tapped transformers are summarized, and the operation mechanisms of the composite system are analyzed in detail. In Section III, controllers are designed to regulate the

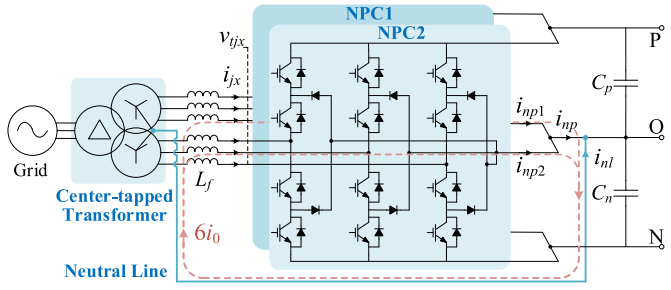

Fig. 3. Proposed dual 3L-NPC converter system for bipolar DC distribution.

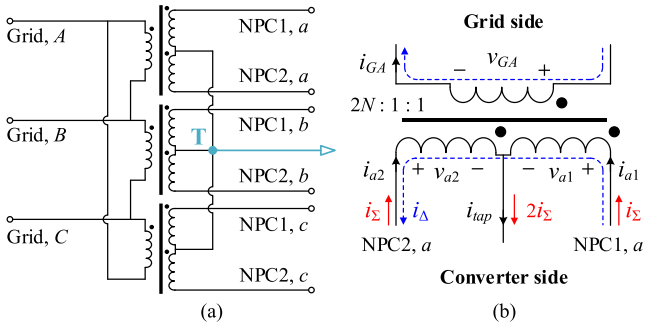

Fig. 4. Center-tapped transformer. (a) Topology and connection diagram. (b) Σ-Δ domain circuit model of phase *a*.

dc-link voltage and balance the dc pole voltages. Simulation and experimental verifications are implemented in Section IV to demonstrate the claimed advantages of the proposed scheme, and to verify the correctness of the theoretical analysis. Finally, Section V concludes this article.

II. Proposed Dual 3L-NPC Converter System

A. Bipolar Distribution System Based on Dual 3L-NPC Converters

The proposed dual 3L-NPC converter system for bipolar dc distribution systems is shown in Fig. 3. A three-phase three-winding transformer with center-tapped connection of the converter-side windings is used as the distribution transformer. The dual 3L-NPC converter arrangement (NPC1 and NPC2) employs grid interface inductances L_f. On the dc side, NPC1 and NPC2 are connected in parallel, and the split dc-link capacitors (C_p and C_n) naturally form the bipolar three-wire structure with P and N denoting positive and negative poles, respectively. The neutral points of the 3L-NPC converters are tied together at the neutral terminal (O) of the bipolar dc link. Importantly, a neutral line connection is added between the center taps of the transformer windings and the dc-side neutral terminal, to provide a flow path for dc-side neutral balancing currents.

Compared to the scheme in Fig. 2(b), the proposed converter system maintains a full bipolar voltage balancing capability, but with a simpler and less costly transformer arrangement. Furthermore, the proposed scheme obtains improved dc-side power quality in terms of reduced ripples through a differential operation of the 3L-NPC converters. Detailed analyses are presented in the following sections to elaborate the above advantages.

B. Features of Center-Tapped Transformer

Transformers with center-tapped windings have been around for decades. The so-called center-tapped transformer is commonly used in the push–pull converter for higher power handling and efficiency, where it is also called a split primary winding transformer [29]. A modular push–pull PWM converter is presented in [30] for applications of battery energy storage systems, which applies a single-phase center-tapped transformer per phase. Additionally, three-phase center-tapped transformers are used for bipolar dc operation by working with 2L-VSC [31] or MMC [32]. In this article, a center-tapped transformer is adopted in the proposed converter system for multiple purposes including power transmission, dc flux cancellation, and bipolar voltage balancing.

The topology and connection diagram of the center-tapped transformer in Fig. 3 are detailed in Fig. 4(a). The grid side windings are connected to the ac grid, and the delta connection is implemented among three windings in order to provide a circulation path for third harmonic currents. The open-ended converter side windings directly connect to the ac terminals of dual 3L-NPC converters, ensuring the simplicity of connection. These windings are segmented in the center of each phase with their center taps combined together at point T, which is then connected with terminal O in the dc side through a dedicated neutral line connection.

To make further analyses, taking phase *a* as an example, a Σ-Δ domain circuit model is presented in Fig. 4(b), where the phase *a* currents of dual 3L-NPC converters can be written as the combination of common mode (CM, Σ) component and differential mode (DM, Δ) component:

$$\begin{cases} i_{a1} = i_\Sigma + i_\Delta \\ i_{a2} = i_\Sigma - i_\Delta \end{cases}. \tag{1}$$

The voltages and currents between the grid side and converter side windings satisfy

$$v_{GA} = 2Nv_{a1} = -2Nv_{a2} \tag{2}$$

$$i_{GA} = (i_{a1} - i_{a2})/2N. \tag{3}$$

According to (1) and (3), the phase *a* current in the grid side can be written as follows:

$$i_{GA} = i_\Delta / N \tag{4}$$

which reveals the first feature of a center-tapped transformer, i.e., DM currents from dual 3L-NPC converters will induce currents in the grid side windings without flowing into the neutral line. Therefore, through modulating dual converters with DM signals, a specific power could be transmitted between grid and converter sides.

The current flowing through center tap of phase *a* winding is calculated as follows:

$$i_{\text{tap}} = i_{a1} + i_{a2} = 2i_\Sigma \tag{5}$$

which reveals the second feature of a center-tapped transformer, i.e., CM currents from dual NPC converters will flow to the center taps without causing transformer saturation, as they will

be cancelled out with each other and produce zero net flux in the core. This is a significant benefit of a center-tapped transformer arrangement.

Given there is a neutral line connecting the point T to the dc terminal O, as shown in Figs. 3 and 4, the CM currents from three center taps will flow into the neutral line:

$$i_{nl} = 3i_{\text{tap}} = 6i_{\Sigma} \tag{6}$$

where i_{nl} is the neutral line current and is helpful to solve the pole voltage imbalance on the dc side [16], [33]. Therefore, by adding CM components into the phase currents of dual 3L-NPC converters, voltage balance of two dc poles can be realized through proper current control, which will be clarified in the following sections.

In summary, the first feature of center-tapped transformer guarantees its function of power transmission by control of DM currents, while the second feature facilitates bipolar voltage balancing without risk of core saturation by control of CM currents. In addition, the technique of employing center-tapped windings is mature and relatively well understood; compared with the zigzag transformers that are relatively less used, the manufacture of center-tapped transformers is considered less complex and costly [32].

C. Analysis of Operation Mechanisms

As shown in Fig. 3, there are two 3L-NPC converters in the proposed converter system. Assuming sinusoidal PWM strategy is applied for the xth ($x = 1, 2$) converter, the averaged ac terminal voltage of phase j ($j = a, b, c$) is

$$v_{tjx}(t) = m_{jx}(t)\frac{V_{\text{dc}}}{2} \tag{7}$$

where V_{dc} is the dc-link voltage; $m_{jx}(t)$ is the phase j modulation signal for the xth converter:

$$m_{jx}(t) = M\cos\left[\omega t + \theta_j + (x-1)\,\pi\right] \tag{8}$$

where M is the modulation index, ω is the angular frequency, and θ_j is the initial phase of phase j modulation signal: $\theta_j = [0, -2\pi/3, 2\pi/3]$ for $j = a, b, c$.

Equation (8) implies the dual 3L-NPC converters have the feature of differential operation, i.e., there is a phase difference of 180° between their modulation signals. This feature not only ensures the power transmission between grid and converter sides, as suggested by (4), but also brings the advantage of improved pole voltages, which will be elaborated later.

Ac terminal currents of the xth converter are written as follows:

$$i_{jx}(t) = I_m\cos\left(\omega t + \theta_j - \varphi + (x-1)\,\pi\right) + i_0 \tag{9}$$

where I_m is the amplitude of ac currents, φ is the angle of voltage leading current, $\cos\varphi$ is the power factor, and i_0 is the injected zero sequence current flowing in each phase.

Based on (6), only the zero sequence components of $i_{jx}(t)$ can flow into the neutral line through the center taps; considering that i_0 is in opposite direction of i_{Σ} in (6), the neutral line current can be rewritten as follows:

$$i_{nl} = -6i_0. \tag{10}$$

Through introducing switching function and average operator [34], the averaged NP current is derived as (11) for phase j of the xth converter

$$i_{npjx}(t) = \left(1 - |m_{jx}(t)|\right) i_{jx}(t). \tag{11}$$

According to Fig. 3, the NP current of the xth converter is calculated as follows:

$$i_{npx}(t) = \sum_{j=a,b,c} i_{npjx}(t) = 3i_0 - \sum_{j=a,b,c} |m_{jx}(t)|\, i_{jx}(t). \tag{12}$$

The composition of $i_{npx}(t)$ is crucial for explaining the operation mechanisms of the proposed converter system and warrants elaboration. To further investigate $i_{npx}(t)$, let

$$f_x(t) = \sum_{j=a,b,c} |m_{jx}(t)|\, i_{jx}(t) = \sum_{j=a,b,c} m_{jx}(t) i_{jx}(t)\text{sgn}(m_{jx}) \tag{13}$$

where sgn(·) is a sign function defined as follows:

$$\text{sgn}(x) = \begin{cases} 1, x > 0 \\ 0, x = 0 \\ -1, x < 0 \end{cases}. \tag{14}$$

sgn(m_{jx}) is a periodic function, which can be expanded by using Fourier series

$$\text{sgn}(m_{jx}) = \frac{4}{\pi}\sum_{k=1}^{\infty}\frac{1}{k}\sin\left(\frac{k\pi}{2}\right)\cos\left[k\left(\omega t + \theta_j\right) + (x-1)\,\pi\right]. \tag{15}$$

Substitute (8), (9), and (15) into (13), and rewrite it as follows:

$$f_x(t) = f_{x\alpha}(t) + f_{x\beta}(t) + f_{x\gamma}(t) \tag{16}$$

where

$$f_{x\alpha}(t) = (-1)^{x+1}\frac{6MI_m}{\pi}\cos\varphi\sum_{k=3,9,15}^{\infty}\frac{1}{k}\sin\left(\frac{k\pi}{2}\right)\cos\left(k\omega t\right)$$

$$f_{x\beta}(t) = (-1)^{x+1}\frac{3MI_m}{\pi}\sum_{k=1,7,13}^{\infty}\frac{1}{k}\sin\left(\frac{k\pi}{2}\right)\times\cos\left[(k+2)\omega t - \varphi\right] + (-1)^{x+1}\frac{3MI_m}{\pi}\sum_{k=5,11,17}^{\infty}\frac{1}{k}\sin\left(\frac{k\pi}{2}\right)\cos\left[(k-2)\omega t + \varphi\right]$$

$$f_{x\gamma}(t) = \frac{6Mi_0}{\pi}\sum_{k=5,11,17}^{\infty}\frac{1}{k}\sin\left(\frac{k\pi}{2}\right)\cos\left[(k+1)\omega t\right] + \frac{6Mi_0}{\pi}\sum_{k=1,7,13,19}^{\infty}\frac{1}{k}\sin\left(\frac{k\pi}{2}\right)\cos\left[(k-1)\omega t\right].$$

The total NP current is the sum of those from NPC1 and NPC2 and can be expressed by using $f_x(t)$

$$i_{\text{np}}(t) = i_{\text{np1}}(t) + i_{\text{np2}}(t) = 6i_0 - \left[f_1(t) + f_2(t)\right]. \tag{17}$$

From (16) and (17), it can be seen that $f_x(t)$ is composed of dc and higher frequency components, which respectively correspond to the dc and harmonics currents of $i_{\text{np}}(t)$. In the following sections, the dc component currents will be analyzed first to explain the bipolar voltage balancing mechanism of the proposed

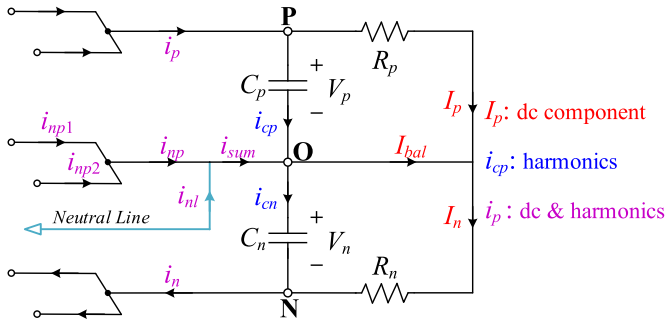

Fig. 5. DC-side analysis circuit of a bipolar DC distribution grid.

converter system; then the low-order harmonic currents will be analyzed to elaborate the advantages of improved dc-side power quality.

1) DC Component Analysis: To analyze the asymmetrical operation of a bipolar dc distribution grid, a dc-side analysis circuit of the proposed converter system is given in Fig. 5. Note that only dc components are considered in this section. For ease of analysis, the unbalanced load condition is denoted by

$$R_p = \varepsilon R_n \tag{18}$$

where R_p and R_n are positive and negative loads, respectively. $\varepsilon \in (0, +\infty)$ is defined as the unbalanced degree.

The converter system in Fig. 3 is able to maintain balanced pole voltages under all the load conditions, i.e.

$$V_p = V_n = \frac{V_{\rm dc}}{2}. \tag{19}$$

To realize the dc voltage balance, the required balancing current from the terminal O is

$$I_{\rm bal} = I_n - I_p = \left(\frac{\varepsilon - 1}{2}\right)\frac{V_{\rm dc}}{R_p}. \tag{20}$$

Note that $I_{\rm bal} = 0$ for $\varepsilon = 1$, which denotes the balanced loads.

It is known from (16) that only $f_{x\gamma}(t)$ has a dc component when $k = 1$, so the dc component of $f_x(t)$ is calculated as follows:

$$F_1 = F_2 = \frac{6M}{\pi} I_0 \tag{21}$$

where I_0 is the dc component of zero sequence current i_0.

From (12) and (21), it is concluded that the dc NP currents of NPC1 and NPC2 are identical:

$$I_{\rm np1} = I_{\rm np2} = \left(3 - \frac{6M}{\pi}\right) I_0. \tag{22}$$

Let the sum current from the dual converters and neutral line supplies the required balancing current

$$I_{\rm np1} + I_{\rm np2} + I_{nl} = I_{\rm bal}. \tag{23}$$

Substituting (10), (20), and (22) into (23), the final equation of the required I_0 is obtained as follows:

$$I_0 = \frac{\pi(1-\varepsilon)}{24M}\frac{V_{\rm dc}}{R_p}. \tag{24}$$

Given that $V_{\rm dc}$ and R_p are known, the required I_0 in Fig. 3 can be determined by (24) for any ε and M. For example, assuming $V_{dc}/R_p = 1$A, the relationship between ε, M, and I_0 is illustrated in Fig. 6.

The injected I_0 flowing through the neutral line and dual converters can ensure the dc voltage balance under any load

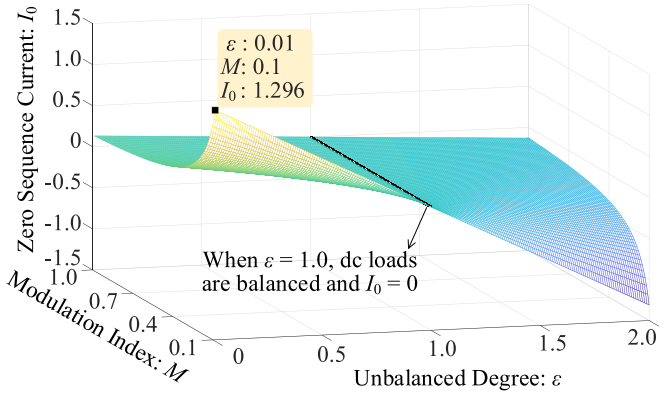

Fig. 6. Required I_0 for $\varepsilon \in (0, 2)$ and $M \in [0.1, 1.0]$.

conditions. This means the system is Fig. 3 can realize full bipolar voltage balancing capability, i.e., each dc pole power flow can be independently controlled. Moreover, the injected I_0 will not cause extra current stress on semiconductor switches or transformer windings; thus, no penalty of increased component ratings is imposed [16], [31].

2) Low-Order Harmonics Analysis: The proposed converter system can achieve improved dc-side power quality without using complex control or modulation strategies. This will be supported by the below analysis. Note that only low-order harmonic components are considered in this section.

According to (16) and (17), all low-order harmonics are cancelled in $i_{np}(t)$ except multiples of the third harmonic, i.e., triple-*n* harmonics. For the *x*th 3L-NPC converter, as shown in (12), the harmonic components of $i_{npx}(t)$ only exist in $f_x(t)$ if the insignificant harmonics in i_0 are neglected. Therefore, the expressions of triple-*n* harmonics in $i_{npx}(t)$ can be obtained by simplifying (16).

For the odd triple-*n* harmonics (3rd, 9th, 15th, etc.), the expression is

$$i_{npx\_\rm odd} = (-1)^x \frac{MI_m}{\pi} \sum_{k=3,9,15}^{\infty} \sin\left(\frac{k\pi}{2}\right)\left[\frac{6\cos\varphi}{k}\cos(k\omega t) - \frac{3}{k-2}\cos(k\omega t - \varphi) - \frac{3}{k+2}\cos(k\omega t + \varphi)\right]. \tag{25}$$

Equation (25) implies the odd triple-*n* harmonics from $i_{\rm np1}(t)$ and $i_{\rm np2}(t)$ are out-of-phase and can be cancelled out with each other in $i_{\rm np}(t)$ according to (17). Recall that the modulation signals for NPC1 and NPC2 given in (8) have a phase difference of 180°, so it is the differential operation of dual converters that realizes the elimination of the odd triple-*n* harmonics in the total NP current.

For the even triple-*n* harmonics (6th, 12th, 18th, etc.), the expression is as follows:

$$i_{npx\_\rm even} = \frac{12Mi_0}{\pi} \sum_{k=6,12,18}^{\infty} \frac{1}{k^2-1}\cos\left(\frac{k\pi}{2}\right)\cos(k\omega t). \tag{26}$$

It can be seen from (26) that the even triple-*n* harmonics from $i_{\rm np1}(t)$ and $i_{\rm np2}(t)$ are in-phase and are accumulated in $i_{\rm np}(t)$.

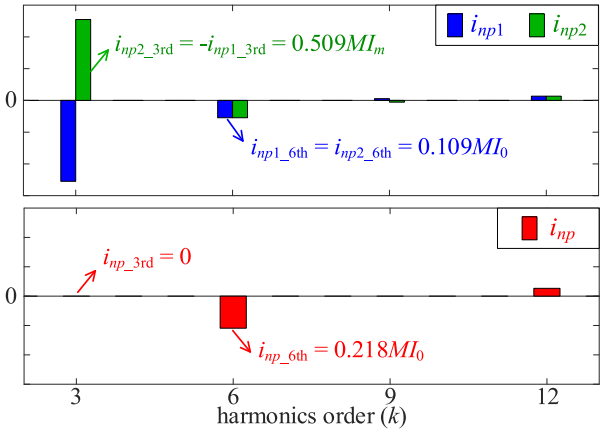

Fig. 7. Low-order harmonics distribution of i_{np1}, i_{np2}, and i_{np}.

Based on (25) and (26), the total NP current from dual converters is rewritten from (17)

$$i_{\rm np} = 6i_0 + \frac{24Mi_0}{\pi}\sum_{k=6,12,18}^{\infty}\frac{1}{k^2-1}\cos\left(\frac{k\pi}{2}\right)\cos\left(k\omega t\right). \tag{27}$$

On the basis of (25)–(27), assuming a unity power factor, the low-order harmonics distribution of $i_{\rm np1}$, $i_{\rm np2}$, and $i_{\rm np}$ is illustrated in Fig. 7. Compared to the NP current offered by a single 3L-NPC converter, the odd triple-n harmonics are eliminated from the total NP current of dual converters, while the even triple-n harmonics are doubled. Considering I_0 is relatively small compared to I_m, the amplitudes of even triple-n harmonics are also quite small. Therefore, the elimination of odd triple-n harmonics, especially the third harmonic, can significantly reduce the ripple of $i_{\rm np}(t)$ and improve its power quality. Moreover, because all the triple-n harmonics are zero sequence components, the elimination of odd triple-n harmonics also decreases the ripple of the zero sequence current i_0 and contributes to a smoother neutral line current according to (10).

For further analysis, consider again the dc-side circuit in Fig. 5 but with only harmonic components. Both the dual converters and neutral line will provide currents to the dc side, and the sum current only consists of even triple-n harmonics according to (10) and (27)

$$i_{\rm sum} = i_{\rm np} + i_{nl} = \frac{24Mi_0}{\pi}\sum_{k=6,12,18}^{\infty}\frac{1}{k^2-1}\cos\left(\frac{k\pi}{2}\right)\cos\left(k\omega t\right) \tag{28}$$

which will flow equally into two dc poles. Therefore, the pole currents can be rewritten as the combination of dc and harmonics components

$$i_p = I_{\rm dc} - i_{\rm sum}/2 \tag{29}$$

$$i_n = I_{\rm dc} + i_{\rm sum}/2 \tag{30}$$

where $I_{\rm dc}$ is the dc current flowing through the dc loads when balanced load condition is assumed. In contrast, harmonics components are mostly flowing through capacitors

$$i_{cp} = -i_{cn} = -i_{\rm sum}/2. \tag{31}$$

TABLE I
COMPARISON OF SCHEMES FOR HIGH-POWER BIPOLAR DC DISTRIBUTION

Converter system	Fig. 2(a)	Fig. 2(b)	Fig. 3 (Proposed)
Full bipolar voltage balancing capability	Yes	Yes	Yes
Transformer	Two conventional transformers	Two zigzag transformers	One center-tapped transformer
Capital cost	Higher	Medium	Lower
Pole voltage ripples	Triple-n harmonics	Triple-n harmonics	Only even triple-n harmonics left
Dc-side power quality	Normal	Normal	Improved

Based on (31), the pole voltages can be rewritten from (19) into the following equations:

$$v_p = \frac{V_{\rm dc}}{2} - \frac{1}{C_p}\int\frac{i_{\rm sum}}{2}dt \tag{32}$$

$$v_n = \frac{V_{\rm dc}}{2} + \frac{1}{C_n}\int\frac{i_{\rm sum}}{2}dt. \tag{33}$$

According to (28)–(33), the harmonic components of i_p, i_n, v_p, and v_n are all related to those of $i_{\rm sum}$. Since odd triple-n harmonics are eliminated from $i_{\rm np}$ and $i_{\rm sum}$, the associated harmonic components will also be removed from the pole currents and voltages, which contributes to reduced ripples and improved power quality.

In summary, due to the differential operation of the dual 3L-NPC converters, odd triple-n harmonics are eliminated from the total NP current in the proposed converter system, thereby achieving ripple reduction in the pole currents and voltages.

D. Comparative Advantages

In order to further clarify the advantages of the proposed converter system in Fig. 3, a qualitative comparison between Figs. 2(a), (b), and 3 is implemented in Table I. As summarized in the table, all three 3L-NPC-related schemes are used for high-power bipolar dc distribution and have a full bipolar voltage balancing capability. However, Fig. 2(a) is using an additional VB for full bipolar voltage balancing, while Fig. 2(b) leaves out the VB by using zigzag transformers to replace the conventional two-winding transformers, and thus has a lower capital cost than Fig. 2(a). Both Fig. 2(a) and (b) are using two transformers and suffer ripple issues in the dc pole voltages. In contrast, the proposed converter system in Fig. 3 uses a center-tapped transformer to replace two zigzag transformers, which not only leads to a lower cost, but also realizes the elimination of odd triple-n harmonics through differential operation between dual converters. As a consequence, the proposed converter system gains a unique advantage of improved dc-side power quality in form of reduced pole voltage ripples.

III. PROPOSED CONTROL STRATEGY

In order to realize the advantages of the proposed converter system in Fig. 3, a double-loop controller is designed in the synchronous reference frame, i.e., dq-frame, in view of its

TABLE II
SPECIAL FEATURES OF THE PROPOSED CONTROL STRATEGY

Controlled object	Control mode	Current reference	Advantage
Zero sequence current	Common-mode control	$i_{0\_ref\_1} = i_{0\_ref\_2}$	Full voltage balancing capability
d-axis current	Differential-mode control	$i_{d\_ref\_1} = -i_{d\_ref\_2}$	Improved dc-side power quality

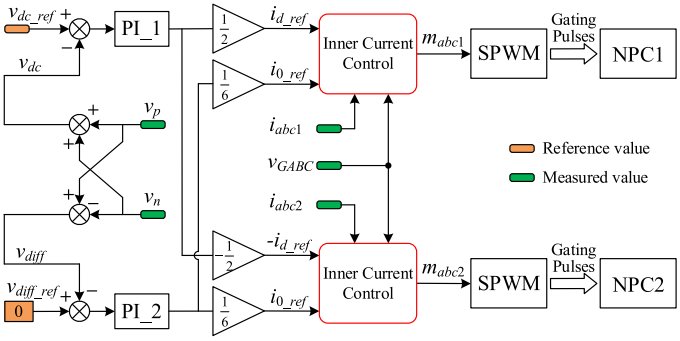

Fig. 8. Block diagram of the proposed control strategy.

advantages in dc quantities tracking and zero steady-state error over the $\alpha\beta$-frame [35]. As summarized in Table II, the proposed converter system has specifically designed features to guarantee its advantages, such as common-mode control for zero sequence current and differential-mode control for d-axis current. In addition to these, the proposed control strategy is relatively simple and utilizes the well-established dq-frame control approach. This simplicity is a salient feature of the proposed converter system. The block diagram of the designed controller is presented in Fig. 8.

The proposed controller measures several input quantities, including ac terminal currents of dual converters (i_{abc1}, i_{abc2}) and dc pole voltages (v_p, v_n). Besides, grid side three-phase voltages (v_{GABC}) are measured as the inputs of phase-locked loop (PLL), which is used for the synchronization of dq-frame.

In the outer voltage loop, $v_{\rm dc}$ and $v_{\rm diff}$ are obtained first as the sum and difference of v_p and v_n, i.e., $v_{\rm dc} = v_p + v_n$ and $v_{\rm diff} = v_p - v_n$. Then, based on two proportional integral (PI) regulators, $v_{\rm dc}$ and $v_{\rm diff}$ are compared with their references ($v_{\rm dc\_ref}$, $v_{\rm diff\_ref}$), with the outputs as follows:

$$i_{d\_\rm ref} = \frac{1}{2}\left(v_{\rm dc\_ref} - v_{\rm dc}\right)\left(K_{\rm p1} + \frac{K_{\rm i1}}{s}\right) \tag{34}$$

$$i_{0\_\rm ref} = \frac{1}{6}\left(v_{\rm diff\_ref} - v_{\rm diff}\right)\left(K_{\rm p2} + \frac{K_{\rm i2}}{s}\right) \tag{35}$$

where $i_{d\_\rm ref}$ and $i_{0\_\rm ref}$ are respectively the references for d-axis current and zero sequence current. To achieve the differential operation of dual converters, d-axis current references for NPC1 and NPC2 are set as opposite. However, $i_{0\_\rm ref}$ for dual converters should always be kept equal to guarantee dc flux cancellation in the transformer core. $K_{\rm p}$ and $K_{\rm i}$ respectively represent the proportion and integration coefficients of the PI regulator.

In the inner current loop, identical controllers (shown in Fig. 9) are used for the 3L-NPC converters. The PLL transforms

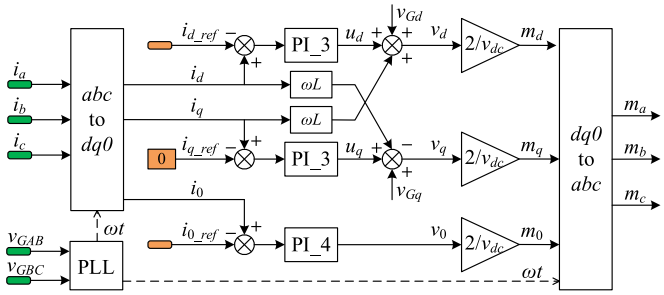

Fig. 9. Block diagram of the inner current controller.

v_{GABC} into v_{Gdq} and obtains the rotational speed ω of the dq-frame, which is used for the park transformation of three-phase currents and modulation signals. i_d, i_q, and i_0 are obtained and compared with their references. Three PI compensators are used to regulate the currents, with control outputs v_d, v_q, and v_0 respectively given by

$$v_d = (i_d - i_{d\_\rm ref})\left(K_{\rm p3} + \frac{K_{\rm i3}}{s}\right) + \omega L i_q + v_{Gd} \tag{36}$$

$$v_q = (i_q - i_{q\_\rm ref})\left(K_{\rm p3} + \frac{K_{\rm i3}}{s}\right) - \omega L i_d + v_{Gq} \tag{37}$$

$$v_0 = (i_0 - i_{0\_\rm ref})\left(K_{\rm p4} + \frac{K_{\rm i4}}{s}\right). \tag{38}$$

Note that $i_{q\_\rm ref}$ is set as zero since the system is assumed to operate at unity power factor, and feedforward signals are added to improve the dynamic response.

Finally, the control signals [v_d, v_q, v_0] from (36)–(38) are scaled down by a factor of $v_{\rm dc}/2$; the obtained [m_d, m_q, m_0] are transformed to the abc-frame and delivered to the PWM generators to generate the gating pulses for 3L-NPC converters. The synchronization of PWM pulses, as a common requirement in practice, is important for the proposed converter system to realize the improved dc-side power quality. Considering a switching frequency of tens of kHz, it is not difficult to synchronize the PWM signals of two converters with mainstream controllers whose frequencies are at least tens of MHz. It should be noted that the zero sequence modulation signal m_0 is generated to counteract the dc voltage drop caused by parasitic resistance, which is very small compared to the dc-link voltage. Therefore, the required m_0 is nearly zero and negligible in practice [16].

IV. VERIFICATION STUDIES

In order to verify the advantages of the proposed dual 3L-NPC converter system, a specific scenario is designed and presented in Table III. It consists of two steps, each of which can demonstrate some features and advantages of the proposed converter system. The system starts in operating at balanced load condition ($R_p = R_n = R_L$, $\varepsilon = 1$), then Step 1 starts at t_1, where the load on the negative pole will be disconnected ($R_p = R_L$, $R_n = \infty$, $\varepsilon = 0$). This step will verify the full bipolar voltage balancing capability of the proposed scheme, whose mechanism has been analyzed in Section II-C. Step 2 starts at t_2, where one 3L-NPC converter (NPC2) fails and system operates on only a single converter

TABLE III
DESIGNED CASE STUDY SCENARIO

Scenario	Step 1	Step 2
Enable time	t_1	t_2
Action	Remove the load on the negative pole.	Block NPC2 and halve the load power.
Load condition	$R_p = R_L$, $R_n = \infty$, $\varepsilon = 0$.	$R_p = 2R_L$, $R_n = \infty$, $\varepsilon = 0$.
Verified advantages	Full bipolar voltage balancing capability.	Improved dc-side power quality.
Related theoretical analysis	Section II-C-1	Section II-C-2
Related verification results	Section IV-A-1 Section IV-B-1	Section IV-A-2 Section IV-B-2

TABLE IV
SIMULATION PARAMETERS

Parameter	Value	Parameter	Value
Grid RMS line voltage	72 kV	DC-link voltage	40 kV
Grid frequency	50 Hz	Switching frequency	5 kHz
Transformer turns ratio	3 : 1 : 1	DC load (R_L)	20 Ω
Filter inductance (L_f)	40 mH	Capacitance per pole	2 mF
Enable time of Step 1 (t_1)	0.25 s	Enable time of Step 2 (t_2)	0.40 s

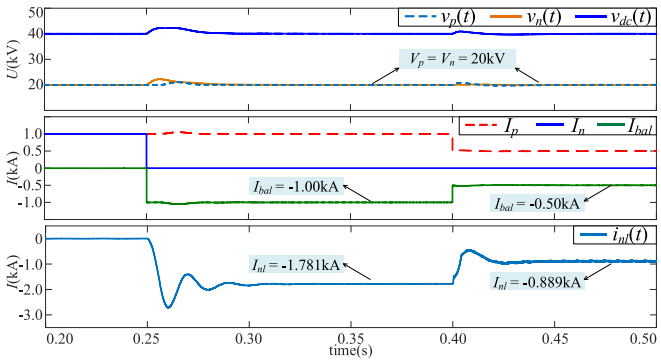

Fig. 10. Simulation waveforms of DC-side voltages and currents.

(NPC1). The load value on the positive pole will double ($R_p = 2R_L, R_n = \infty, \varepsilon = 0$) to halve load power; otherwise, the currents flowing through NPC1 will exceed the ratings. Through the waveforms comparison between dual-converter operation and single-converter operation, the improved dc-side power quality in terms of ripple reduction enabled by the proposed scheme will be demonstrated.

A. Simulation Results

The proposed scheme is firstly verified by means of simulation. An MVDC distribution system of the structure shown in Fig. 3 is modeled in MATLAB/Simulink. The simulation parameters are listed in Table IV.

1) Full Bipolar Voltage Balancing Capability: The designed scenario in Table III is implemented for the system model, and the simulation waveforms of dc-side voltages and currents are presented in Fig. 10. With the proposed converter system and control strategy, when the dc loads become completely unbalanced at $t_1 = 0.25$ s, both the dc-link voltage ($v_{\rm dc}$) and the pole voltages (v_p, v_n) of the MVDC distribution system remain stable after a short transient, which reflects a strong and full capability of balancing dc pole voltages. Additionally, the dc component of negative pole current (I_n) drops to zero immediately and the required balancing current ($I_{\rm bal}$) complies with (20). Owing to the addition of a neutral line, the zero sequence currents (i_0) can flow through the dual converters and form neutral line current (i_{nl}), then their dc components can provide the $I_{\rm bal}$ needed for dc voltage balancing.

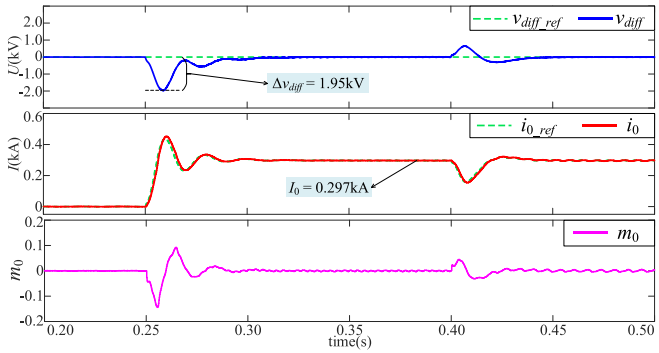

Fig. 11. Simulation waveforms showing dynamic performance of the controller.

The dynamic performance of the proposed control strategy is shown in Fig. 11. When R_n is disconnected at t_1, the differential voltage ($v_{\rm diff}$) can be regulated to the zero reference in less than 0.05 s, with an overshoot less than 2 kV (5% of $v_{\rm dc}$). This is benefited from the fast tracking of $i_{0\cdot\rm ref}$, which is enabled by the inner loop of i_0. It should be noted that the dc value of zero sequence currents ($I_0 = 0.297$ kA) is in good agreement with (24), and the relationship between I_{nl} and I_0 is also in accord with (10). In addition, m_0 has a small transient overshoot and a nearly zero steady-state value, which has negligible effect to the modulation process. All of the above results validate the effectiveness and fast dynamic characteristic of the designed controller.

2) Improved DC-Side Power Quality: According to the designed scenario in Table III, NPC2 is blocked at $t_2 = 0.40$ s, which means the system operation before and after t_2 is based on dual converters and single converter, respectively. Hence, the special advantages (e.g., improved dc-side power quality) of the proposed dual-converter system can be verified through comparing the system performances before and after t_2.

The pole voltages and currents waveforms around t_2 are enlarged in Fig. 12(a) for observation and comparison. Two time spans (TS1 and TS2) are selected before and after t_2, which represent dual-converter operation and single-converter operation, respectively. Fast Fourier transform (FFT) analysis is implemented during TS1 and TS2, and the low-order harmonics distribution results are presented in the right side. Compared to TS1, odd triple-n harmonics appear during TS2, and large third harmonics can be observed in v_p and v_n, which explains the noticeable ripples in the pole voltages. The third harmonics in v_p and v_n are caused by those in i_p and i_n, and the relationships between their amplitudes are in good accord with (32) and (33).

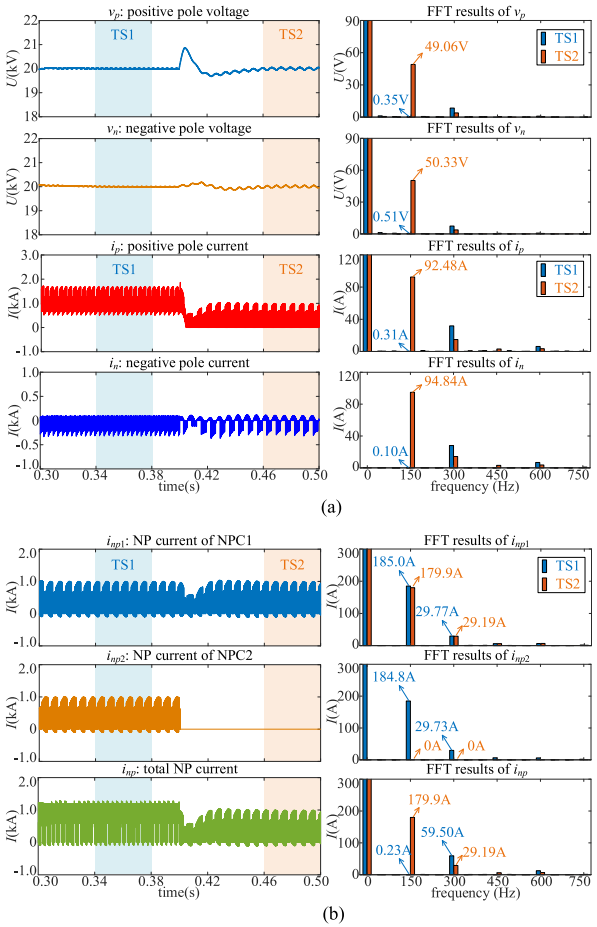

Fig. 12. Simulation waveforms to verify improved DC-side power quality. (a) Pole currents, pole voltages and their FFT analysis results. (b) NP currents and their FFT analysis results.

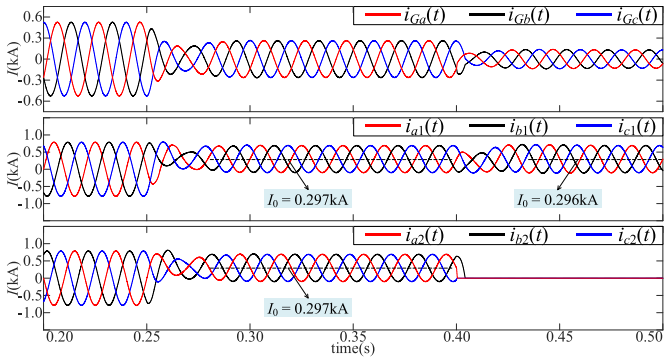

Fig. 13. Simulation waveforms of the three-phase AC currents.

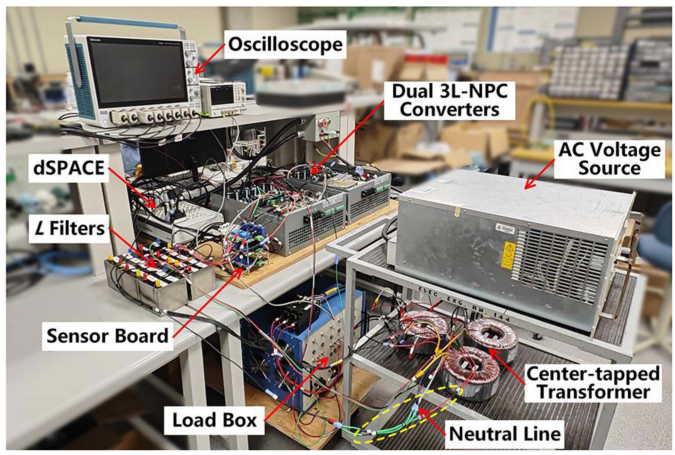

Fig. 14. Photograph of the experimental setup.

According to the analysis related to (25), it is the differential operation of dual converters that realize the elimination of the odd triple-n harmonics in the NP current (i_{np}), thereby improving the power quality of pole currents and voltages.

In order to further verify the veracity of previous theoretical analysis, the NP currents waveforms enlarged around t_2 and their FFT results are given in Fig. 12(b). During TS1, i_{np1} and i_{np2} have equal but opposite odd triple-n harmonics, which are nullified in the total i_{np} of dual converters, while the remaining even triple-n harmonics are added in i_{np}. In contrast, i_{np2} becomes zero during TS2, so all the triple-n harmonics from single converter will be observed in i_{np}, leading to a deteriorated waveform. The harmonics distribution of i_{np} matches well with (27). For example, the sixth harmonic of i_{np} has a simulated amplitude of 59.50 A during TS1, while according to Fig. 7, its theoretical value is calculated as 60.21 A for $M = 0.930$ and $I_0 = 0.297$ kA.

3) AC-Side Currents: The simulation waveforms of three-phase ac currents are presented in Fig. 13. When NPC2 is blocked at t_2, the proposed dual-converter system becomes a single-converter system. The amplitudes of grid currents (i_{Gabc}) are reduced by half due to the halved load power. Three-phase ac currents of NPC2 (i_{abc2}) become zero, while those of NPC1 (i_{abc1}) remain stable after an instant, which will not exceed the original component ratings. The required I_{bal} reduces to half because of the halved load, but the injected I_0 of NPC1 remains the original value, as it is the only contributor for dc voltage balancing at the moment. Considering the core saturation of the center-tapped transformer, the proposed converter system cannot operate on the basis of a single converter for a long time. More studies are needed for eliminating the risk of core saturation during single-converter operation.

B. Experimental Results

An experimental setup, as shown in Fig. 14, is built in the laboratory and used to further support the simulation results. A three-phase programmable ac power supply is used to emulate the ac grid. The three-phase center-tapped transformer is built by connecting three single-phase transformers in the manner shown in Fig. 4(a). A neutral line is realized by connecting the dc neutral terminal to the center taps of the individual transformers. The dSPACE MicroLabBox DS1202 is used as the controller.

The designed scenario in Table III is implemented again in this downscaled experimental setup, which can emulate a low voltage dc (LVDC) distribution system. The main system parameters are listed in Table V.

1) Full Bipolar Voltage Balancing Capability: Fig. 15 presents the experimental waveforms of dc-side voltages and

TABLE V
EXPERIMENTAL SYSTEM PARAMETERS

Parameter	Value	Parameter	Value
Grid RMS line voltage	208 V	DC-link voltage	200 V
Grid frequency	50 Hz	Switching frequency	5 kHz
Transformer turns ratio	2.18 : 1 : 1	DC load (R_L)	14.4 Ω
Filter inductance (L_f)	5 mH	Capacitance per pole	580 μF

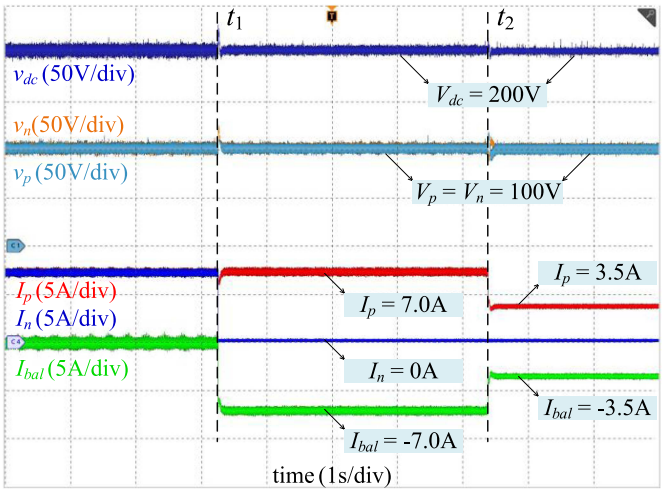

Fig. 15. Experimental DC-side voltage and current waveforms validating full voltage balancing capability.

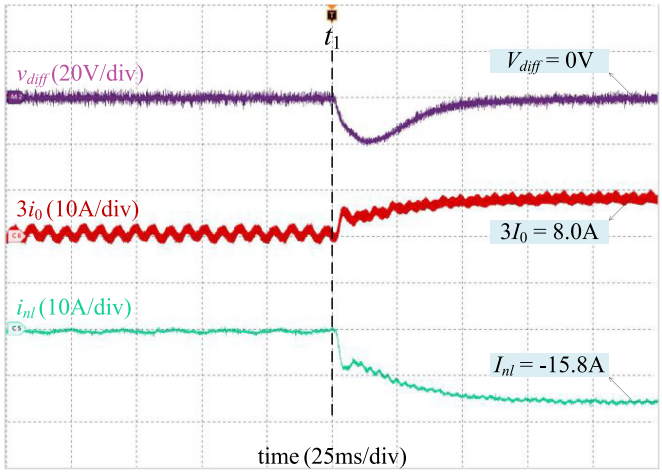

Fig. 16. Experimental dynamic performance of the designed controller.

currents. For the entire time span of 10 s, including Step 1 at t_1 and Step 2 at t_2, $v_{\rm dc}$ remains close to its reference value and v_p maintains balance with v_n, which validates the full voltage balancing capability of the proposed scheme as well as the effectiveness of the designed control strategy. With the changes of loading conditions shown in Table III, the values of I_p, I_n, and $I_{\rm bal}$ also change accordingly.

Fig. 16 shows the waveforms of $v_{\rm diff}$, i_0, and i_{nl} captured around t_1. After the sudden disconnection of R_n, there is a transient of less than 0.1 s, which demonstrates the fast dynamic characteristic of the designed controller. All steady-state values

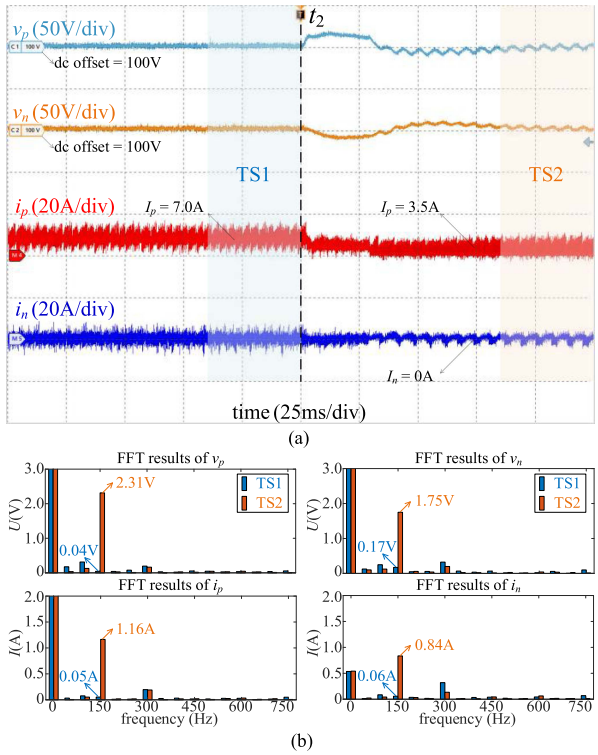

Fig. 17. Experimental results of the pole voltages and currents verifying the improved DC-side power quality. (a) Experimental waveforms. (b) FFT analysis results.

are consistent with the theoretical values, and the relationship between I_0 and I_{nl} properly corresponds to (10).

2) Improved dc-Side Power Quality: Fig. 17(a) presents the experimental waveforms of pole voltages and currents captured around t_2. Still, TS1 and TS2 are selected before and after t_2 respectively to represent dual-converter operation and single-converter operation. It is evident that the waveforms during TS2 have more low-order harmonics compared to those during TS1. FFT analysis is implemented for a further clarification of harmonics distribution. As shown in Fig. 17(b), large third harmonics can be observed for v_p and v_n during TS2, which are the primary causes of voltage ripples and are consequences of third harmonics appearing in i_p and i_n. Conversely, for waveforms during TS1, third harmonics are almost eliminated due to the differential operation of dual converters, which corresponds to the analysis regarding (25). In a word, the proposed dual-converter system successfully achieves improved pole voltages of reduced ripples compared to single-converter systems.

3) AC-Side Currents: Fig. 18(a) displays the 10-s waveforms of the three-phase currents from dual 3L-NPC converters. For the Step 1, i_{abc1} and i_{abc2} are halved due to the disconnection of R_n. After Step 2, i_{abc2} becomes zero as NPC2 is blocked, while i_{abc1} maintains the previous values because it is NPC1 that processes all the transmitted power of the LVDC distribution system though the power is reduced by half. Besides, the injected I_0 are 2.7 A for both converters before t_2. This value holds for NPC1 after t_2, because NPC1 individually provides the balancing current to the dc side. A center-tapped transformer

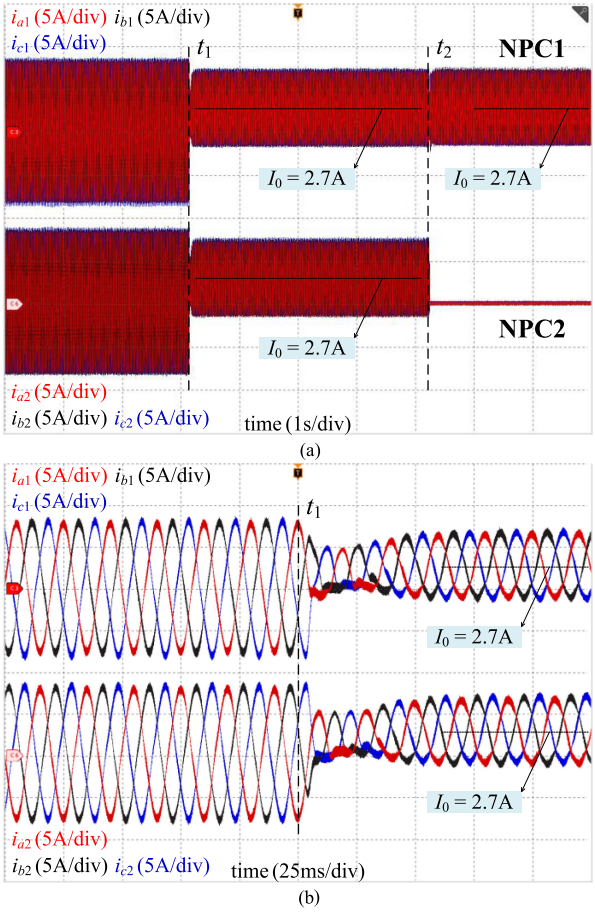

Fig. 18. Experimental AC-side current waveforms of dual 3L-NPC converters. (a) 10-s waveforms. (b) Enlarged view around t_1.

will suffer the core saturation problem during single-converter operation. A zigzag transformer, however, doesn't have such risks due to its complex structure. With only a center-tapped transformer, the proposed converter system gains lower cost and improved power quality, but suffers a risk of transformer saturation when one converter fails. This is a tradeoff to some degree.

Fig. 18(b) enlarges the three-phase currents waveforms around t_1. It is observed that i_{abc1} and i_{abc2} have a phase difference of 180°, which reflects the differential operation feature of the proposed scheme. As analyzed in Section II-C, this feature is the key to simultaneously realize the power transmission and bipolar dc voltage balancing. The equal distribution of I_0 in dual converters (both equal to 2.7 A) is also essential, because it can prevent the saturation problem for center-tapped transformers, as analyzed in Section II-B. Besides, the peak values of i_{abc1} and i_{abc2} do not exceed their rated values even under the most unbalanced condition, which validates the feature of zero penalty on component ratings. In summary, for the proposed scheme, it is the combination of differential operation, zero sequence current injection, and the features of center-tapped transformers that concurrently realizes the functions of power transmission and dc voltage balancing.

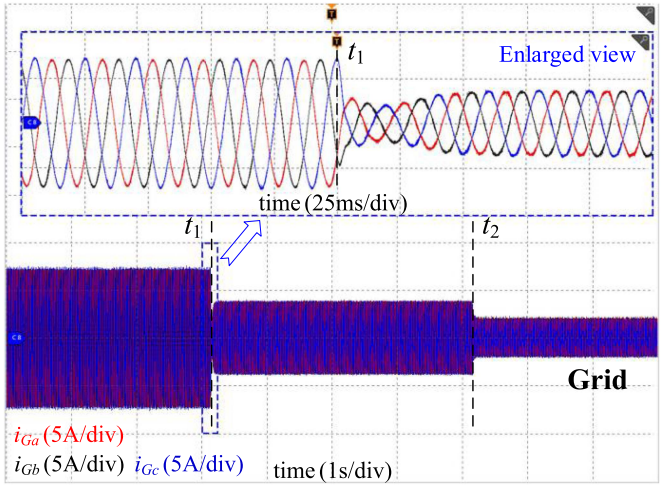

Fig. 19. Experimental AC current waveforms of the grid side and its enlarged view around t_1.

Fig. 19 presents the experimental ac current waveforms in the grid side. It can be found that the amplitude of i_{Gabc} is halved at t_1 since the dc load power is reduced by half, and halved again at t_2 due to the doubled R_p. There is no dc offset in i_{Gabc} because I_0 will not flow through the grid side. An enlarged view of the ac current waveforms around t_1 is given. A short transient can be watched for i_{Gabc} when the dc load condition changes, and the waveforms of i_{Gabc} generally keep smooth all the time, which validates that the dc load change does not have significant adverse effects on the grid-side ac currents.

V. Conclusion

This article presents a dual 3L-NPC converter system for high-power bipolar dc distribution, which offers additional advantages compared to the existing schemes. First, benefiting from the manipulation of zero sequence currents and the use of a center-tapped transformer, the proposed scheme gains full bipolar voltage balancing capability without resorting to the use of multiple zigzag transformers. Second, the odd multiples of third harmonic can be eliminated from the NP current by virtue of the differential operation of dual 3L-NPC converters, thereby achieving improved dc-side power quality in terms of ripple reduction. This is not possible to achieve when using multiple single converters in parallel, as with prior art. To verify the advantages of the proposed scheme, a specific scenario is designed, which is implemented for an MVDC distribution system in simulations and an LVDC distribution system in experiments. Both the simulation and experimental results validate that the proposed scheme can 1) maintain the bipolar voltage balancing under completely unbalanced load conditions; and 2) improve the dc-side power quality by reducing the ripples in the pole voltages and currents. The verification results also show good consistency with theoretical analysis results.

References

[1] T. Dragičević, P. Wheeler, and F. Blaabjerg, "Bipolar-type DC microgrids for high-quality power distribution," in *DC Distribution Systems and Microgrids*. London, U.K.: Inst. Eng. Technol., 2018, pp. 245–266.

[2] Y. Li, F. Nejabatkhah, and H. Tian, "Renewable energy, energy storage, and smart interfacing power converters," *Smart Hybrid AC/DC Microgrids: Power Management, Energy Management, and Power Quality Control*. Hoboken, NJ, USA: Wiley, 2022, pp. 21–54.
[3] B. Grainger and R. De Doncker, "Power electronic converters impacts on MVDC system architectures," in *Medium Voltage DC System Architectures*. London, U.K.: Inst. Eng. Technol., 2021, pp. 19–94.
[4] CIGRE WG C6/B4.37, "Introduction," in *Medium Voltage DC Distribution Systems*, Tech. Brochure, vol. 875. Paris, France: CIGRE, 2022, pp. 9–15.
[5] T. Kaipia, P. Salonen, J. Lassila, and J. Partanen, "Possibilities of the low voltage DC distribution systems," in *Proc. Nordac, Nordic Distrib. Asset Manage. Conf.*, 2006, pp. 1–10.
[6] G. V. D. Broeck, W. Martinez, M. Dalla Vecchia, S. Ravyts, and J. Driesen, "Conversion efficiency of the buck three-level DC–DC converter in unbalanced bipolar DC microgrids," *IEEE Trans. Power Electron.*, vol. 35, no. 9, pp. 9306–9319, Sep. 2020.
[7] R. Teichmann and S. Bernet, "A comparison of three-level converters versus two-level converters for low-voltage drives, traction, and utility applications," *IEEE Trans. Ind. Appl.*, vol. 41, no. 3, pp. 855–865, May/Jun. 2005.
[8] L. Tan, B. Wu, S. Rivera, and V. Yaramasu, "Comprehensive DC power balance management in high-power three-level DC–DC converter for electric vehicle fast charging," *IEEE Trans. Power Electron.*, vol. 31, no. 1, pp. 89–100, Jan. 2016.
[9] A. Choudhury, P. Pillay, and S. S. Williamson, "Discontinuous hybrid-PWM-based DC-link voltage balancing algorithm for a three-level neutral-point-clamped (NPC) traction inverter drive," *IEEE Trans. Ind. Appl.*, vol. 52, no. 4, pp. 3071–3082, Jul./Aug. 2016.
[10] S. Rivera, W. Bin, S. Kouro, V. Yaramasu, and J. Wang, "Electric vehicle charging station using a neutral point clamped converter with bipolar DC bus," *IEEE Trans. Ind. Electron.*, vol. 62, no. 4, pp. 1999–2009, Apr. 2015.
[11] S. Rivera and B. Wu, "Electric vehicle charging station with an energy storage stage for split-DC bus voltage balancing," *IEEE Trans. Power Electron.*, vol. 32, no. 3, pp. 2376–2386, Mar. 2017.
[12] H. Aburub, J. Holtz, J. Rodriguez, and G. Baoming, "Medium-voltage multilevel converters-state of the art, challenges, and requirements in industrial applications," *IEEE Trans. Ind. Electron.*, vol. 57, no. 8, pp. 2581–2596, Aug. 2010.
[13] S. Kouro et al., "Recent advances and industrial applications of multilevel converters," *IEEE Trans. Ind. Electron.*, vol. 57, no. 8, pp. 2553–2580, Aug. 2010.
[14] J. Yu, K. Smith, M. Urizarbarrena, N. MacLeod, R. Bryans, and A. Moon, "Initial designs for the ANGLE DC project; converting existing AC cable and overhead line into DC operation," in *Proc. 13th IET Int. Conf. AC DC Power Transmiss.*, 2017, pp. 1–6.
[15] J. Chen, W. Ming, C. E. Ugalde-Loo, S. Wang, and N. Jenkins, "Analysis and mitigation of DC voltage imbalance for medium-voltage cascaded three-level neutral-point-clamped converters," *IEEE Trans. Power Electron.*, vol. 37, no. 4, pp. 4320–4336, Apr. 2022.
[16] B. Li, H. Tian, L. Ding, X. Wu, G. J. Kish, and Y. R. Li, "An improved three-level neutral point clamped converter system with full-voltage balancing capability for bipolar low-voltage DC grid," *IEEE Trans. Power Electron.*, vol. 38, no. 12, pp. 15792–15803, Dec. 2023.
[17] L. Tan, B. Wu, V. Yaramasu, S. Rivera, and X. Guo, "Effective voltage balance control for bipolar-DC-bus-fed EV charging station with three-level DC–DC fast charger," *IEEE Trans. Ind. Electron.*, vol. 63, no. 7, pp. 4031–4041, Jul. 2016.
[18] S. Cui, J.-H. Lee, J. Hu, R. W. De Doncker, and S.-K. Sul, "A modular multilevel converter with a zigzag transformer for bipolar MVDC distribution systems," *IEEE Trans. Power Electron.*, vol. 34, no. 2, pp. 1038–1043, Feb. 2019.
[19] Y.-R. Kim, S.-Y. Lee, S. Cui, and J.-J. Jung, "Improvement of DC voltage control dynamics with bipolar DC circuits using a zigzag transformer," in *Proc. 24th Int. Conf. Elect. Mach. Syst.*, 2021, pp. 2060–2064.
[20] J.-S. Hong, J.-I. Ha, S. Cui, and J. Hu, "Topology and control of an enhanced dual-active bridge converter with inherent bipolar operation capability for LVDC distribution systems," *IEEE Trans. Power Electron.*, vol. 38, no. 10, pp. 12774–12789, Oct. 2023.
[21] J. Shen, S. Schroder, B. Duro, and R. Roesner, "A neutral-point balancing controller for a three-level inverter with full power-factor range and low distortion," *IEEE Trans. Ind. Appl.*, vol. 49, no. 1, pp. 138–148, Jan./Feb. 2013.
[22] T.-K.-T. Nguyen, N.-V. Nguyen, and N. R. Prasad, "Eliminated commonmode voltage pulsewidth modulation to reduce output current ripple for multilevel inverters," *IEEE Trans. Power Electron.*, vol. 31, no. 8, pp. 5952–5966, Aug. 2016.
[23] C. Xia, G. Zhang, Y. Yan, X. Gu, T. Shi, and X. He, "Discontinuous space vector PWM strategy of neutral-point-clamped three-level inverters for output current ripple reduction," *IEEE Trans. Power Electron.*, vol. 32, no. 7, pp. 5109–5121, Jul. 2017.
[24] X. Xing, X. Li, F. Gao, C. Qin, and C. Zhang, "Improved space vector modulation technique for neutral-point voltage oscillation and commonmode voltage reduction in three-level inverter," *IEEE Trans. Power Electron.*, vol. 34, no. 9, pp. 8697–8714, Sep. 2019.
[25] J.-S. Lee and K.-B. Lee, "Time-offset injection method for neutral-point AC ripple voltage reduction in a three-level inverter," *IEEE Trans. Power Electron.*, vol. 31, no. 3, pp. 1931–1941, Mar. 2016.
[26] Y. Zhang, J. Li, X. Li, Y. Cao, M. Sumner, and C. Xia, "A method for the suppression of fluctuations in the neutral-point potential of a three-level NPC inverter with a capacitor-voltage loop," *IEEE Trans. Power Electron.*, vol. 32, no. 1, pp. 825–836, Jan. 2017.
[27] F. Chen, W. Qiao, H. Wang, and L. Qu, "A simple zero-sequence voltage injection method for carrier-based pulsewidth modulation of the three-level NPC inverter," *IEEE J. Emerg. Sel. Topics Power Electron.*, vol. 9, no. 4, pp. 4687–4699, Aug. 2021.
[28] N. Celanovic and D. Boroyevich, "A comprehensive study of neutralpoint voltage balancing problem in three-level neutral-point-clamped voltage source PWM inverters," *IEEE Trans. Power Electron.*, vol. 15, no. 2, pp. 242–249, Mar. 2000.
[29] N. Mohan, T. M. Undeland, and W. P. Robbins, "Switch-Mode dc-ac Inverters: dc ↔ Sinusoidal ac," in *Power Electronics: Converters, Applications, and Design*, 3rd ed. Hoboken, NJ, USA: Wiley, 2003, pp. 200–248.
[30] M. Hagiwara and H. Akagi, "Experiment and simulation of a modular push–pull PWM converter for a battery energy storage system," *IEEE Trans. Ind. Appl.*, vol. 50, no. 2, pp. 1131–1140, Mar./Apr. 2014.
[31] C. Perera, J. Salmon, and G. J. Kish, "Multiport converter with independent control of AC and DC power flows for bipolar DC distribution," *IEEE Trans. Power Electron.*, vol. 36, no. 3, pp. 3473–3485, Mar. 2021.
[32] Y. Li, D. Liu, and G. J. Kish, "A dual-MMC chain-link structure for multifrequency power transfer," *IEEE Trans. Power Electron.*, vol. 37, no. 12, pp. 14601–14614, Dec. 2022.
[33] J. Lago and M. L. Heldwein, "Operation and control-oriented modeling of a power converter for current balancing and stability improvement of DC active distribution networks," *IEEE Trans. Power Electron.*, vol. 26, no. 3, pp. 877–885, Mar. 2011.
[34] A. Yazdani and R. Iravani, "Three-level, three-phase, neutral-point clamped, voltage-sourced converter," in *Voltage-Sourced Converter in Power Systems: Modelling, Control, and Application*, Hoboken, NJ, USA: Wiley, 2010.
[35] T. M. Rowan and R. J. Kerkman, "A new synchronous current regulator and an analysis of current-regulated PWM inverters," *IEEE Trans. Ind. Appl.*, vol. IA-22, no. 4, pp. 678–690, Jul. 1986.

Bowei Li (Graduate Student Member, IEEE) received the B.S. and M.S. degrees in electrical engineering from Shandong University, Jinan, China, in 2017 and 2020, respectively. He is currently working toward the Ph.D. degree in energy system in the Department of Electrical and Computer Engineering, University of Alberta, Edmonton, AB, Canada.

His research interests include topology, control and power quality of the dc distribution system.

Xuesong Wu (Graduate Student Member, IEEE) received the B.Eng. (Yisheng Mao Honors) and M.Sc. degrees in electrical engineering from Southwest Jiaotong University, Chengdu, China, in 2016 and 2019, respectively. He is currently working toward the Ph.D. degree in energy system with the Department of Electrical and Computer Engineering, University of Alberta, Edmonton, AB, Canada.

His research interests include the electrical machine drives and grid-tied inverters.

Gregory J. Kish (Senior Member, IEEE) received the B.E.Sc. degree from the University of Western Ontario, London, ON, Canada, in 2009, and the M.A.Sc. and Ph.D. degrees from the University of Toronto, Toronto, ON, Canada, in 2011 and 2016, respectively, all in electrical engineering.

He is currently an Associate Professor with the University of Alberta, Edmonton, AB, Canada. His research interests include the development and application of power electronic converter systems in electric grids.

Yunwei Ryan Li (Fellow, IEEE) is a professor, University of Alberta Senior Engineering Research Chair, and Chair of the Department of Electrical and Computer Engineering.

He received the B.Sc. in Engineering degree in electrical engineering from Tianjin University, Tianjin, China, in 2002, and the Ph.D. degree in electrical engineering from Nanyang Technological University, Singapore, in 2006. In 2005, Dr. Li was a Visiting Scholar with Aalborg University, Denmark. From 2006 to 2007, he was a Postdoctoral Research Fellow at the Toronto Metropolitan University, Canada. In 2007, he also worked at Rockwell Automation Canada before he joined University of Alberta, Canada in the same year. His research interests include distributed generation, microgrid, renewable energy, high power converters and electric motor drives.

Dr. Li is the Vice President for Products of IEEE Power Electronics Society (PELS) 2022–2024. He was the Editor-in-Chief for IEEE TRANSACTIONS ON POWER ELECTRONICS LETTERS 2019–2023. Prior to that, he was Associate Editor for IEEE TRANSACTIONS ON POWER ELECTRONICS, IEEE TRANSACTIONS ON INDUSTRIAL ELECTRONICS, IEEE TRANSACTIONS ON SMART GRID, and IEEE JOURNAL OF EMERGING AND SELECTED TOPICS IN POWER ELECTRONICS. Dr. Li served as the general chair of IEEE Energy Conversion Congress of Exposition (ECCE) in 2020 for the first ever virtual version during the pandemic. Dr. Li received the Nagamori Foundation Award in 2022 and the Richard M. Bass Outstanding Young Power Electronics Engineer Award from IEEE PELS in 2013. He is a Fellow of the Canadian Academy of Engineering, and recognized as a Highly Cited Researcher by the Clarivate Analytics.